Investigating the Inconsistency of Ionospheric ROTI Indices Derived from GPS Modernized L2C and Legacy L2 P(Y) Signals at Low-Latitude Regions

Zhe Yang, Zhizhao Liu (✉)

Department of Land Surveying and Geo-Informatics, The Hong Kong Polytechnic University

11 Yuk Choi Road, Hung Hom, Kowloon, Hong Kong, P. R. China

Tel. (852)2766 5961 Fax: (852)2330 2994

E-mail: lszzliu@polyu.edu.hk

Abstract: The rate of change of total electron content (TEC) index (ROTI), an important parameter to characterize ionospheric irregularities and associated scintillation activities, can be calculated from both new Global Positioning System (GPS) civilian L2C and legacy GPS L2 P(Y) signals. We investigate the inconsistency of the ROTI indices derived from the L2C, denoted as $ROTI_{L2C}$, and from the L2 P(Y), denoted as $ROTI_{L2P}$, through the analysis of three months of GPS data collected by four types of GNSS receivers, i.e., Javad, Leica, Septentrio and Trimble, installed at five low-latitude stations. The results show that inconsistencies existent between the $ROTI_{L2C}$ and $ROTI_{L2P}$ may be related to the receiver configurations, such as tracking techniques. For both Leica and Trimble receivers, $ROTI_{L2C}$ and $ROTI_{L2P}$ are generally comparable; for the Septentrio receiver, $ROTI_{L2C}$ is larger than $ROTI_{L2P}$ by 0.5 to 1.1 TECu/min; for the Javad receiver, $ROTI_{L2C}$ is smaller than $ROTI_{L2P}$ by -0.5 to 0.3 TECu/min. A significant inconsistency of $ROTI_{L2C}$ (also $ROTI_{L2P}$) is also found from the cross-comparison between the receivers deployed at zero/short baselines. In addition we find that large discrepancy of ROTI is observed for satellites with low maximum elevation angle. Correlation coefficients between $ROTI_{L2C}$ and S_4 are on average in the range of 0.4 to 0.8, comparable to those of $ROTI_{L2P}$ with S_4. But low correlation coefficient is found for satellites with low maximum elevation angle. The ratios between $ROTI_{L2C}$ and S_4 are also calculated. They are in the range of 3 to 9, larger than those between $ROTI_{L2P}$ and S_4. This study suggests that cautions be taken when ROTI index, either $ROTI_{L2P}$ or $ROTI_{L2C}$, derived from different types of GNSS receivers is used to characterize ionospheric irregularities and associated scintillations.

Keywords: Global Positioning System; L2C signal; Rate of Total Electron Content Index; Ionospheric Irregularities and Scintillations

Introduction

As a major part of the ongoing Global Positioning System (GPS) modernization, new civil signals on L1, L2 and L5 frequencies are added to the satellite constellation. These additional civil signals on multiple carrier frequencies provide the capability to enhance the overall performance of the GPS system, in terms of improving signal acquisition and tracking performance, providing better atmospheric corrections and better immunity to radio frequency interference and multipath (Tran 2004; Engel 2008).

As a part of modernization program, L2 civil signal (L2C) on 1227.6 MHz is the first modernized GPS signal for civilians. This new signal was first broadcast on September 25, 2005 by the first GPS Block IIR-M satellite (Leveson 2006). Since then, every GPS satellite launched subsequently has the L2C signal transmission capability. Until 2016, there have been 18 GPS satellites including both Block IIR-M and Block IIF generations in operation transmitting the L2C signal. As the second civilian GPS signal, L2C provides better performance than the current L1 C/A signal, because of its advanced signal structure (Fontana et al. 2001). The combination of L2C with the legacy L1 C/A provides a convenient way for ionospheric error correction and enables a more robust and accurate determination of ionosphere total electron content (TEC) (McDonald 2002; Shanmugam et al. 2012). Tracked at full power and without signal encryption issue, the L2C signal outperforms the legacy L2 P(Y) signal which is also available to civil users but through semi-codeless or similar techniques only (Al-Fanek et al. 2007; Sükeová et al. 2007).

With the increase of the number of L2C-capable GPS modernized satellites, several analyses have been conducted to investigate the performance of L2C signal in aspects of signal to noise ratio and multipath levels (Al-Fanek et al. 2007; Sükeová et al. 2007), and the differential code bias of L2C (Montenbruck et al. 2014a; Wang et al. 2016). In addition, some attentions have been particularly paid to study the performance of L2C measurements in GPS-based applications. Taking advantage of the L2C measurements from a limited number of modernized satellites, Leandro et al. (2008) analyzed the quality of L2C-based code measurements and its impact on precise point positioning (PPP) performance. That analysis indicated that the L2C signal is more easily tracked than L2 P(Y) signal and

L2C brings a minor improvement to the PPP solutions. O'Keefe et al. (2009) as well as Wang and O'Keefe (2010) evaluated the benefit of using L2C measurements to provide an ionospheric correction for standalone GPS positioning and for ambiguity resolution, respectively. Their conclusions suggested that the use of L2C measurements in conjunction with the L1 C/A ones is effective for ionospheric delay estimation. Sokolovskiy et al. (2014) demonstrated that utilizing L2C signal can improve GPS radio occultation inversions in the neutral atmosphere by mainly increasing the total number of processed occultations and by a marginal reduction of noise in statistics. Marques et al. (2015) found that under weak ionospheric scintillation the L2C performance is better than that of L2 P(Y) in performing GPS positioning at the equatorial region of Brazil, while L2C does not contribute to positioning accuracy improvement under strong ionospheric scintillation conditions. Previous studies have clearly shown the contribution of L2C to various GPS-based applications.

L2C has the potential to generate benefits for dual-frequency applications (Leveson 2006). As one of the important applications, GPS dual-frequency observations can be used to characterize ionospheric irregularities via TEC variations (Beach and Kintner 1999). In the past, many indices have been derived from TEC to study the ionospheric irregularities at equatorial and high latitude regions (Oladipo and Schüler 2013; Tiwari et al. 2013, and references therein). The rate of change of TEC index (ROTI) proposed by Pi et al. (1997) is widely used to characterize the presence of ionospheric irregularities and associated scintillations of GPS signals. For instance, Basu et al. (1999) pointed out that the ROTI can be used as an indicator of small-scale ionospheric irregularities causing scintillations. The ROTI is normally derived from the dual-frequency GPS legacy signals, namely L1 C/A and L2 P(Y). So far no study has been conducted to investigate the performance of L2C signal in characterizing ionospheric irregularities and scintillations in conjunction with the L1 C/A signal. In view of this, this study is carried out to evaluate the performance of L2C in estimating TEC derived index to characterize ionospheric irregularities and associated scintillations.

In this study, L2C measurements recorded by one Septentrio Global Navigation Satellite System (GNSS) receiver with PolaRxS Pro model installed at Hong Kong and four GNSS receivers in the Multi-GNSS Experiment (MGEX) network are analyzed (Montenbruck et al. 2014b). These GNSS receivers of different types are all situated at low latitudes where ionospheric irregularities and scintillations are frequently observed (Oladipo and Schüler 2013).

The data and method adopted in the analysis are described first. Thereafter, the performance of L2C data recorded by different types of GNSS receivers to characterize ionospheric irregularities and

scintillations in low latitude regions are analyzed and discussed. Finally, the conclusions are given. The findings of this work will allow us to understand the contribution of the new civilian L2C measurements from different types of GNSS receivers to GNSS-based ionospheric studies.

Data and Method

This section describes the data from different types of GNSS receivers used for the analysis, the estimation of TEC derived index and how the performance of L2C measurements is analyzed.

Data source

The Multi-GNSS Experiment (MGEX) network initiated by the International GNSS Service (IGS) in 2012 serves as a platform for an early familiarization with the emerging new GNSS signals and systems (Rizos et al. 2013). By the end of 2014, more than 120 GNSS stations have been installed within the MGEX network around the world (Wang et al. 2016). These stations are equipped with a wide variety of GNSS receivers, such as Javad, Leica, Trimble and Septentrio, and are capable of tracking GNSS signals from the GPS and GLONASS systems as well as the new GNSS systems, e.g., Beidou and Galileo. Within the MGEX network, some GNSS receivers are deployed to form zero baselines (multiple receivers connecting to a common antenna) or short baselines. This enables a direct comparison of the tracking behavior of the receivers and facilitates the assessment of differential code biases for individual GNSS signals (Montenbruck et al. 2014b). In this study, we will take advantage of four MGEX stations at zero/short baselines to investigate the performance of L2C measurements in studying ionospheric irregularities at low latitude regions. In addition to four stations from the MGEX network, one GNSS-based ionospheric scintillation monitoring station installed at Hok Tsui, Hong Kong is also used.

A brief summary of the selected GNSS stations is given in Table 1 and their locations are shown in Figure 1. As can be seen, two MGEX stations named KOUG and KOUR are equipped with a Leica GR10 receiver and a Septentrio PolaRx4 receiver, respectively, and they are very closely to the magnetic equator. The other two MGEX stations named SIN0 and SIN1 are collocated stations and they are equipped with a Javad TRE-G3TH DELTA receiver and a Trimble NetR9 receiver, respectively. The GNSS-based scintillation monitoring station named HKHT is located at Hong Kong and it is equipped with a Septentrio PolaRxS Pro receiver, which can output GNSS measurements to

characterize the intensity of ionospheric irregularities and associated scintillations (Yang and Liu 2015). Equipped with five models of GNSS receivers produced by four manufacturers, these five GNSS stations offer the same type of GPS legacy measurements, i.e., C/A and P(Y) code on L1 and L2 frequencies, but different types of L2C measurements.

Table 1 Summary of location, receiver model, and observation type of five GNSS stations used in this study

Station	Lat. (°)	Lon. (°)	Geomagnetic Lat. (°)	Receiver type	GPS observation types
HKHT	22.20	114.25	12.38	Septentrio PolaRxS Pro	L1 C/A, L2 P(Y), L2C (L)
KOUG	5.10	-52.64	14.22	Leica GR10	L1 C/A, L2 P(Y), L2C (M)
KOUR	5.25	-52.81	14.38	Septentrio PolaRx4	L1 C/A, L2 P(Y), L2C (L)
SIN0	1.34	103.68	-8.4	Javad TRE-G3TH DELTA	L1 C/A, L2 P(Y), L2C (M+L)
SIN1	1.34	103.68	-8.4	Trimble NetR9	L1 C/A, L2 P(Y), L2C (M+L)

Table 1 shows that three kinds of L2C code measurements are tracked, i.e. the medium length L2C (M) code (Leica), the long length L2C (L) code (Septentrio) and the combined L2C (M+L) signal (Javad and Trimble). The L2C (M) code, which is 20 msec long and contains 10,230 chips, provides short acquisition time and it is modulated by navigation data. The L2C (L) code, which has a period of 1.5 sec and contains 767,250 chips, offers better correlation (Fontana et al. 2001). The L2C (M) code and L2C (L) code play the data and pilot roles, respectively, in a L2C-enabled receiver (Li and Lu 2015). In this study, L2C (M), L2C (L) and L2C (M+L), are analyzed, allowing a cross-comparison of the performances among these three types of L2C measurements.

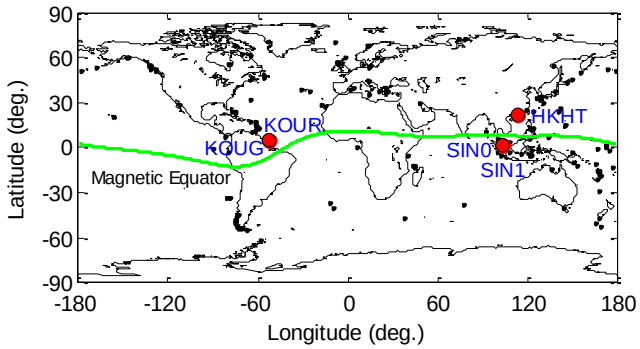

Fig. 1 Geographic distribution of the four GNSS stations (KOUG and KOUR, SIN0 and SIN1) from the MGEX network, and the GNSS-based ionospheric scintillation monitoring station (HKHT) at Hong Kong. The green line represents the magnetic equator.

TEC derived index

Rate of change of total electron content (TEC) index (ROTI), as a TEC derived index, can be obtained from the time rate of differential phase of dual frequency GPS signals (Pi et al. 1997). The estimation of ROTI starts from the dual-frequency GPS phase equations including the frequency dependent ionospheric refraction shown as below (Leick et al. 2015):

$$\begin{aligned} \lambda_1 L_1 &= \rho + \lambda_1 N_1 + c\delta_r - c\delta^s - \Delta_1^{ion} + T - d_1 + \varepsilon \\ \lambda_2 L_2 &= \rho + \lambda_2 N_2 + c\delta_r - c\delta^s - \Delta_2^{ion} + T - d_2 + \varepsilon \end{aligned} \quad (1)$$

where λ_1 and λ_2 are the wavelengths at the frequency f_1 and f_2, respectively; L_1 and L_2 are the corresponding carrier phase measurements; ρ is the geometric distance between receiver and satellite; N_1 and N_2 are the corresponding integer carrier phase ambiguity; c is the speed of light in vacuum; δ_r and δ^s are the receiver and satellite clock bias, respectively; Δ_1^{ion} and Δ_2^{ion} denote the phase delay of GPS signals at the frequency f_1 and f_2 in the ionosphere, respectively; T is the tropospheric delay; d_1 and d_2 are the receiver and satellite hardware phase delays at two frequencies; ε represents other error terms comprising multipath and receiver noise. The phase ionospheric delays Δ_1^{ion} and Δ_2^{ion} can be represented as (Leick et al. 2015):

$$\begin{aligned} \Delta_1^{ion} &= \frac{40.3}{f_1^2} TEC \\ \Delta_2^{ion} &= \frac{40.3}{f_2^2} TEC \end{aligned} \quad (2)$$

Substituting (2) into (1) and forming the difference between $\lambda_2 L_2$ and $\lambda_1 L_1$ can yield TEC:

$$TEC = \frac{1}{40.3}\left(\frac{f_1^2 f_2^2}{f_2^2 - f_1^2}\right)[(\lambda_2 L_2 - \lambda_1 L_1) - (\lambda_2 N_2 - \lambda_1 N_1) + (d_2 - d_1)] \quad (3)$$

The differential TEC observable gives the rate of change of TEC (ROT, in the unit of TECu/min, 1 TECu= 10^{16} electrons/m^2) over the period of interest, as shown below:

$$ROT = \frac{TEC(i) - TEC(i-1)}{(t_i - t_{i-1})} \quad (4)$$

$$ROT = \frac{1}{40.3}\left(\frac{f_1^2 f_2^2}{f_2^2 - f_1^2}\right)\frac{[(\lambda_2 L_2(i) - \lambda_1 L_1(i)) - (\lambda_2 L_2(i-1) - \lambda_1 L_1(i-1))]}{(t_i - t_{i-1})} \quad (5)$$

where $(t_i - t_{i-1})$ is the time difference between the epochs i and i-1. As shown in (5), the initial carrier phase ambiguity and hardware phase delay are cancelled and only the dual-frequency phase terms are left. Defined as the standard deviation of the ROT over a time interval, the ROTI is then calculated as follows (Pi et al. 1997):

$$ROTI = \sqrt{\langle ROT^2 \rangle - \langle ROT \rangle^2} \quad (6)$$

According to (6), ROTI is estimated from 1 Hz dual-frequency GPS phase data over each 5-min period in this study.

Before the estimation of ROTI, the data preprocess is made to detect and repair cycle slips in the dual-frequency phase data based on the method proposed by Liu (2011). In the analysis, two types of ROTI are calculated. One uses phase observations of the legacy signals, i.e., L1 C/A and L2 P(Y), and the other uses phase observations from L1 C/A and L2C signals. The corresponding ROTI are named as $ROTI_{L2P}$ and $ROTI_{L2C}$, respectively.

Analysis method

The dual-frequency GPS data, i.e., legacy L1 and L2 measurements and new civilian L2C measurements collected in the period of July 1 to September 30, 2014 at a sample rate of 1 second are used in this study. During this period, 13 modernized GPS satellites are capable of broadcasting the new civilian L2C signal. Their PRNs are 01, 05, 06, 07, 12, 15, 17, 24, 25, 27, 29, 30 and 31. Their corresponding space vehicle numbers (SVNs) are 63, 50, 67, 48, 58, 55, 53, 65, 62, 66, 57, 64 and 52. Among them, PRNs 05, 07, 12, 15, 17, 29 and 31 (SVNs 50, 48, 58, 55, 53, 57 and 52) are Block IIRM satellites, while PRNs 01, 06, 24, 25, 27 and 30 (SVNs 63, 67, 65, 62, 66 and 64) are Block IIF

satellites. This analysis focuses on these modernized GPS satellites only and only satellite signals with elevation angle 30° or higher are considered in the analysis.

The performance of L2C measurements in characterizing ionospheric irregularities and scintillations is evaluated in terms of $ROTI_{L2C}$ via a comparison with the $ROTI_{L2P}$ derived from the legacy P(Y) code. First, the L2C measurements from the ionospheric scintillation monitoring receiver HKHT at Hong Kong are used to characterize the ionospheric irregularities and associated scintillations. The correlation between $ROTI_{L2C}$ and the amplitude scintillation index S_4 is analyzed, following the work presented in Yang and Liu (2015) which discussed the correlation between ROTI from legacy dual-frequency GPS phase data and ionospheric scintillations indices for low-latitude regions. Thereafter, the L2C measurements from the four MGEX stations equipped with different types of receivers are used to characterize the ionospheric irregularities.

Analysis Results and Discussions

This section presents the analysis results and discussion of the performance of L2C measurements from the GNSS receiver installed at Hong Kong and the four GNSS receivers in the MGEX network in characterizing ionospheric irregularities and scintillations for low latitude regions.

Analysis of L2C measurements from the GNSS scintillation monitoring receiver

The GNSS-based ionospheric scintillation monitoring receiver installed at Hong Kong provides GPS measurements to characterize both ionospheric irregularities and associated scintillations. In order to show temporal variations under non-scintillation and scintillation conditions, Figure 2 displays the ROT, ROTI, and S_4 of all GPS satellites observed on July 18 and September 10, 2014, respectively. The ROT and ROTI are derived from both L2C and L2 P(Y) signals in conjunction with the L1 C/A signal. The S_4 is calculated as the standard deviation of GPS L1 signal intensity amplitude normalized by its mean value over 60 s. In the figures the ROT, ROTI and S_4 values for the modernized GPS satellites are displayed in colors according to the color bar, while the results of other non-modernized GPS satellites are displayed in black.

Under both non-scintillation and scintillation conditions, as indicated in Figure 2, the ROT and ROTI corresponding to the L2C signal, i.e., ROT_{L2C} and $ROTI_{L2C}$, are inconsistent with those from the

legacy L2 P(Y) signal, i.e., ROT_{L2P} and $ROTI_{L2P}$. Figure 2 indicates that ROT_{L2C} and $ROTI_{L2C}$ have larger values than the ROT_{L2P} and $ROTI_{L2P}$, respectively. Under non-scintillation condition, the $ROTI_{L2C}$ can be as large as 1.6 TECu/min, which is significantly larger than $ROTI_{L2P}$. Most $ROTI_{L2P}$ are below 0.4 TECu/min. Under the scintillation condition, both $ROTI_{L2C}$ and $ROTI_{L2P}$ disturb remarkably with respect to the enhancement of scintillation activity in the period of 20:00-2:00 local time and the $ROTI_{L2C}$ is still larger than the $ROTI_{L2P}$.

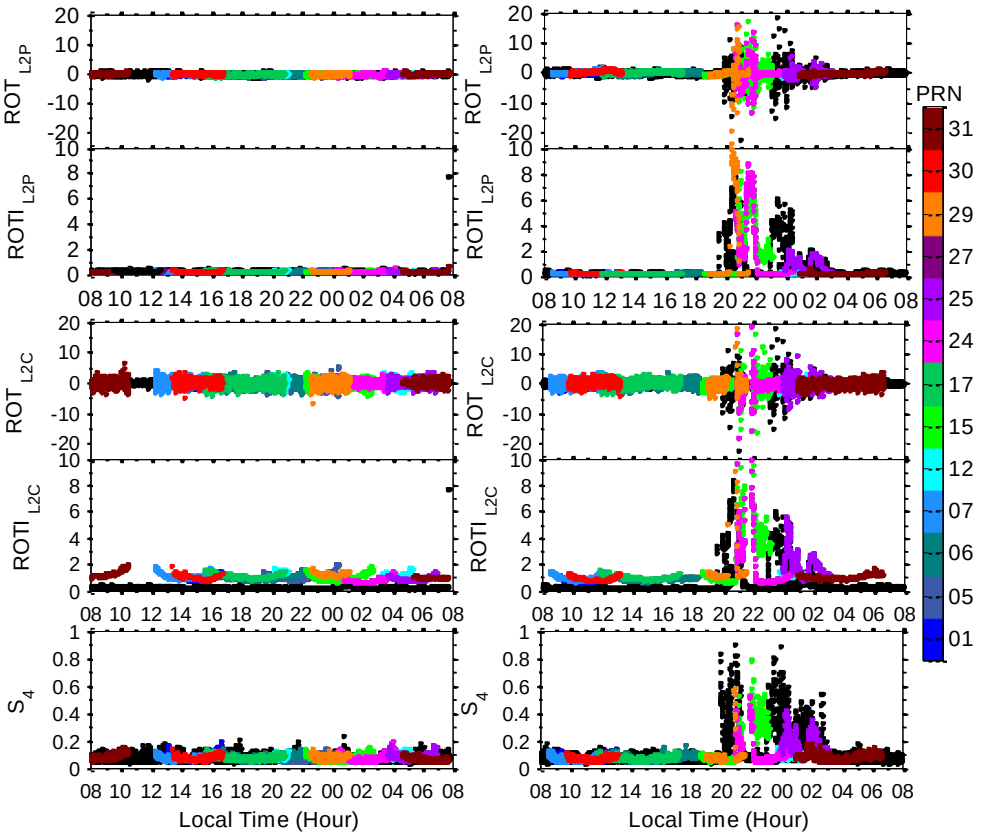

Fig. 2 ROT, ROTI and S_4 derived from GPS data of all satellites collected by the Septentrio PolaRxS Pro GNSS ionospheric scintillation monitoring receiver installed at Hong Kong on July 18, 2014 (left column) and September 10, 2014 (right column). The unit of ROT and ROTI is TECu/min. The values for the modernized GPS satellites (PRNs 01, 05, 06, 07, 12, 15, 17, 24, 25, 27, 29, 30, 31, and corresponding SVNs are 63, 50, 67, 48, 58, 55, 53, 65, 62, 66, 57, 64 and 52) are denoted according to the color bar and the values for other non-modernized GPS satellites are denoted in black.

The ROT, ROTI and S_4 for all the modernized GPS satellites observed in the whole study period July 1 to September 30, 2014 are illustrated in Figure 3. It is clearly observed that both ROT_{L2C} and

$ROTI_{L2C}$, shown in the right column of Figure 3, have remarkably large magnitudes compared with ROT_{L2P} and $ROTI_{L2P}$, in the left column, over the three-month period. In general, the ROT_{L2C} and $ROTI_{L2C}$ are in the ranges of -4 to 4 TECu/min and 0.5 to 1.6 TECu/min, respectively. The ROT_{L2P} and $ROTI_{L2P}$ however vary in the ranges of -1.2 to 1.2 TECu/min and 0.2 to 0.4 TECu/min, respectively. In the presence of amplitude scintillations, as indicated by $S_4 > 0.2$, they all increase with the increase of S_4 and the $ROTI_{L2C}$ can even exceed 6 TECu/min. Overall, the $ROTI_{L2C}$ have larger magnitudes but the variation of $ROTI_{L2C}$ agrees well with that of $ROTI_{L2P}$ as well as S_4.

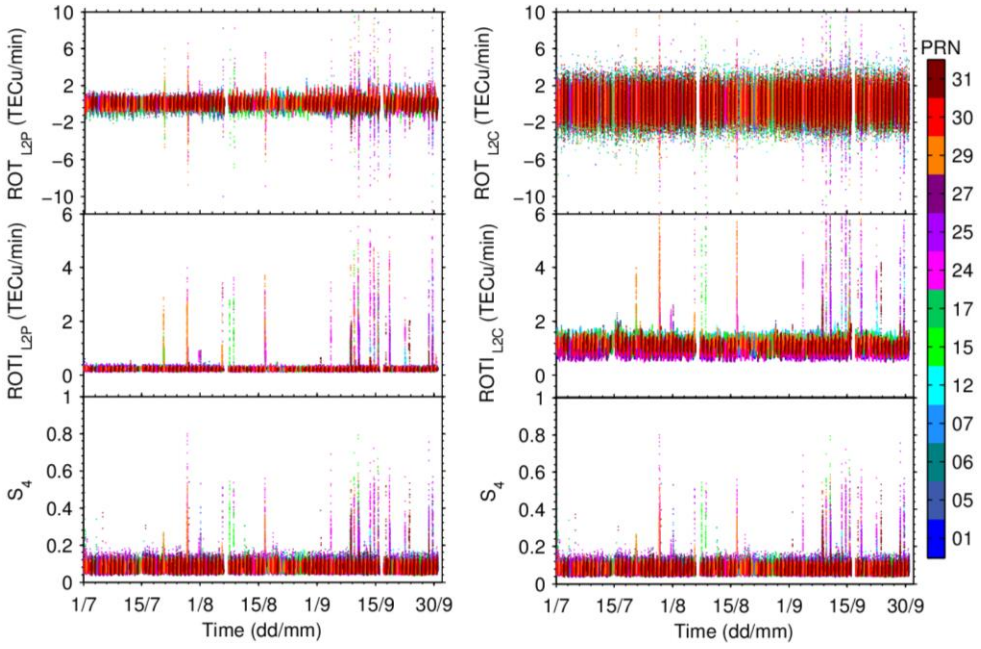

Fig. 3 ROT_{L2P}, $ROTI_{L2P}$ and S_4 (left column) and ROT_{L2C}, $ROTI_{L2C}$ and S_4 (right column) derived from GPS data of modernized satellites collected by the Septentrio PolaRxS Pro GNSS ionospheric scintillation monitoring receiver installed at Hok Tsui of Hong Kong in the period of July 1 to September 30, 2014.

The histogram of the differences between $ROTI_{L2C}$ and $ROTI_{L2P}$ derived from each modernized satellite is given in Figure 4 in order to quantify the overestimation of ROTI made by the new civilian L2C signal. The mean of ($ROTI_{L2C}$-$ROTI_{L2P}$) calculated from each dataset is displayed in each sub-figure. Figure 4 clearly shows that ($ROTI_{L2C}$-$ROTI_{L2P}$) has a bias for each satellite. It shows that the level of $ROTI_{L2C}$ overestimation is normally less than 1 TECu/min for each modernized satellite, and occasionally it can be larger than 3 TECu/min. On average, the bias between $ROTI_{L2C}$ and $ROTI_{L2P}$ is in the range of 0.57 to 1.04 TECu/min.

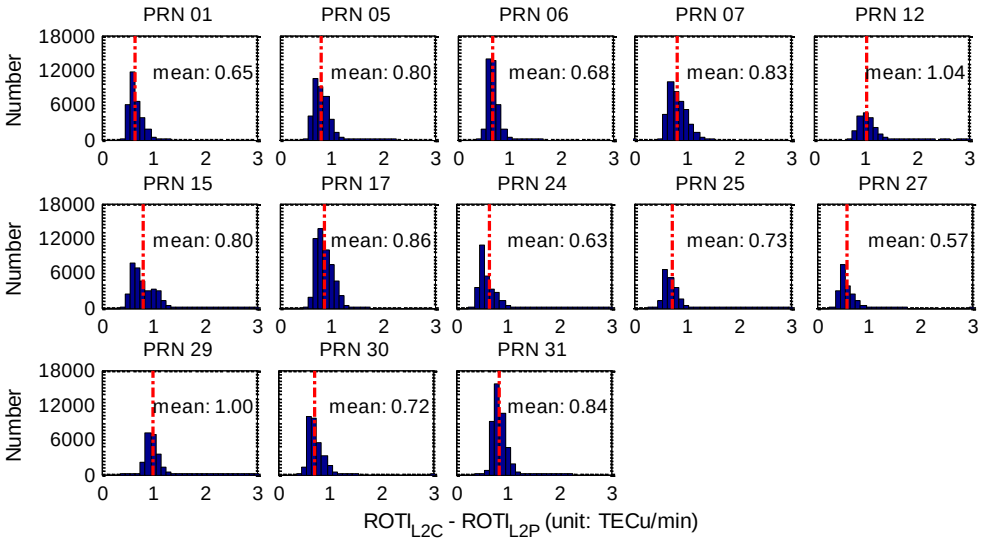

250

251 **Fig. 4** Histogram of (ROTI$_{L2C}$-ROTI$_{L2P}$) of each modernized GPS satellite observed by the Septentrio PolaRxS
252 Pro GNSS ionospheric scintillation monitoring receiver installed at Hok Tsui of Hong Kong in the period of July
253 1 to September 30, 2014. The red dashed line denotes the mean value of (ROTI$_{L2C}$-ROTI$_{L2P}$).

254 The ROTI can be used to predict the presence of ionospheric scintillations induced by ionospheric
255 irregularities (Basu et al. 1999). The recent study by Yang and Liu (2015) shows that the ROTI$_{L2P}$
256 derived from dual-frequency GPS legacy phase data has a high correlation with the scintillation indices,
257 suggesting the feasibility of using ROTI to characterize ionospheric scintillations. In this study, the
258 correlation between ROTI$_{L2C}$ and S_4 is also carried out, in addition to the correlation between ROTI$_{L2P}$
259 and S_4.

260

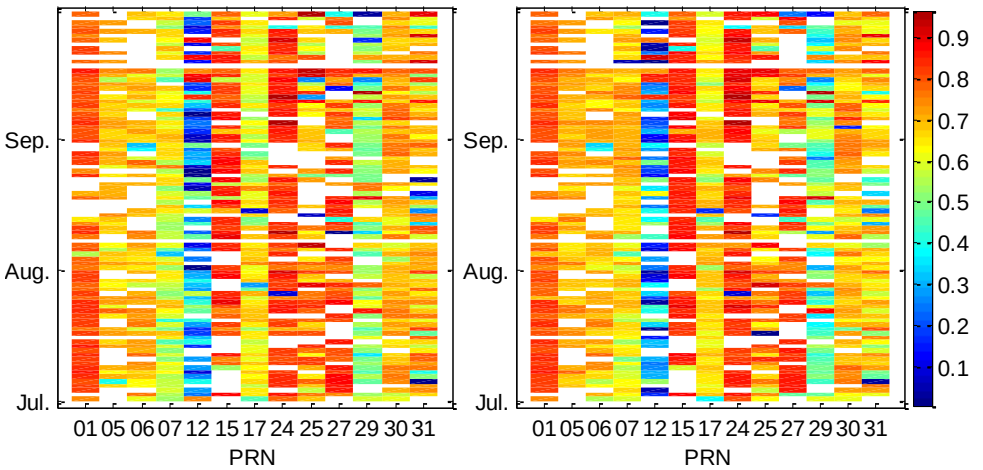

261

262 **Fig. 5** Diurnal correlation coefficient between ROTI$_{L2P}$ and S_4 (Left), ROTI$_{L2C}$ and S_4 (Right) derived from
263 observations of each modernized GPS satellite observed by the Septentrio PolaRxS Pro GNSS ionospheric

scintillation monitoring receiver installed at the Hok Tsui of Hong Kong in the period of July 1 to September 30, 2014. The colors in the bar represent different levels of correlation.

Figure 5 depicts the diurnal correlation coefficient between $ROTI_{L2C}$ ($ROTI_{L2P}$) and S_4 for each modernized satellite over the study period. In general, the correlation level is high and the coefficient is above 0.6 for most satellites. On average, the correlation level of $ROTI_{L2C}$ with S_4 is in the range of 0.4 to 0.8. The maximum $ROTI_{L2C}$ correlation coefficient reaches 0.96 for PRN 24 on September 7, 2014. For both $ROTI_{L2C}$ and $ROTI_{L2P}$, a relatively low correlation is observed for the satellites PRN 12 and PRN 29. To investigate the reason for low correlation, Figure 6 shows the maximum elevation angle, average correlation level and the ratio of ROTI/S_4 for each modernized satellite. The weak correlation between $ROTI_{L2C}$ ($ROTI_{L2P}$) and S_4 for satellites PRN 12 and PRN 29 is found to be related to the low elevation angles of the two satellites. This has also been discussed in Yang and Liu (2015). Because of the large magnitude of $ROTI_{L2C}$ (see Figures 3 and 4), the ratio of $ROTI_{L2C}$ to S_4 is in the range of 3 to 9, which is much larger than that of $ROTI_{L2P}$ to S_4 in the range of 1 to 4.

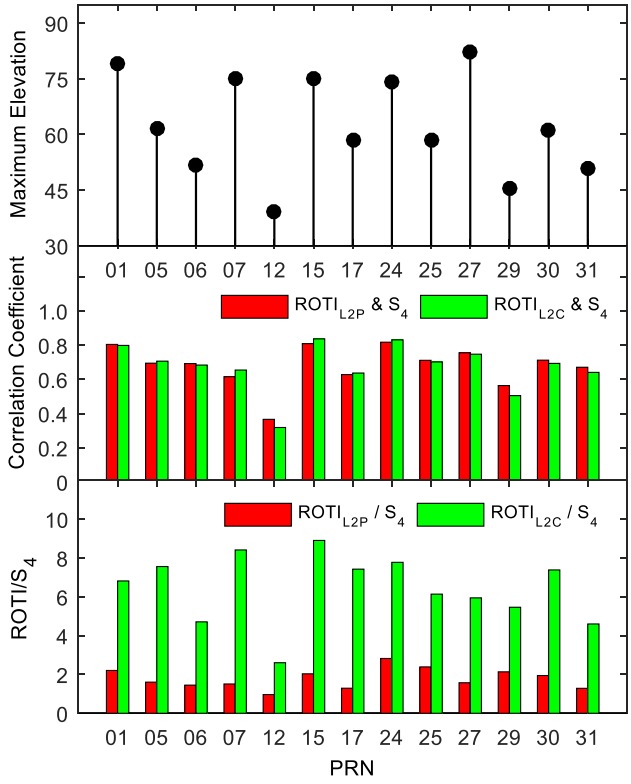

Fig. 6 Maximum elevation angle (top), average correlation coefficient between ROTI and S_4 (middle), and average ratio of ROTI/S_4 (bottom) for each modernized GPS satellite observed by the Septentrio PolaRxS Pro

GNSS ionospheric scintillation monitoring receiver installed at the Hok Tsui of Hong Kong in the period of July 1 to September 30, 2014.

Analysis of L2C measurements from the GNSS receivers in MGEX network

The four GNSS receivers in the MGEX network make GPS measurements using a common antenna or two adjacently installed antennas, which allows a direct comparison of the performance of L2C measurements from different kinds of GNSS receivers in characterizing ionospheric irregularities. As given in Table 1, the stations KOUR and KOUG form a short baseline and the collocated stations SIN0 and SIN1 share one common antenna.

The ROT and ROTI derived from 1-second modernized GPS dual-frequency carrier phase data at the KOUG and KOUR stations for the period July 1 to September 30, 2014, are shown in Figure 7. The results illustrate that both ROT_{L2C} and $ROTI_{L2C}$ have large values in September when ionospheric irregularities occur frequently at the equatorial regions (Oladipo and Schüler 2013). For the ROT_{L2P} and $ROTI_{L2P}$, KOUG and KOUR stations have a very similar level. The ROT_{L2P} and $ROTI_{L2P}$ at the KOUG station are in the range of -1.2 to 1.2 TECu/min and 0.2 to 0.4 TECu/min, respectively.

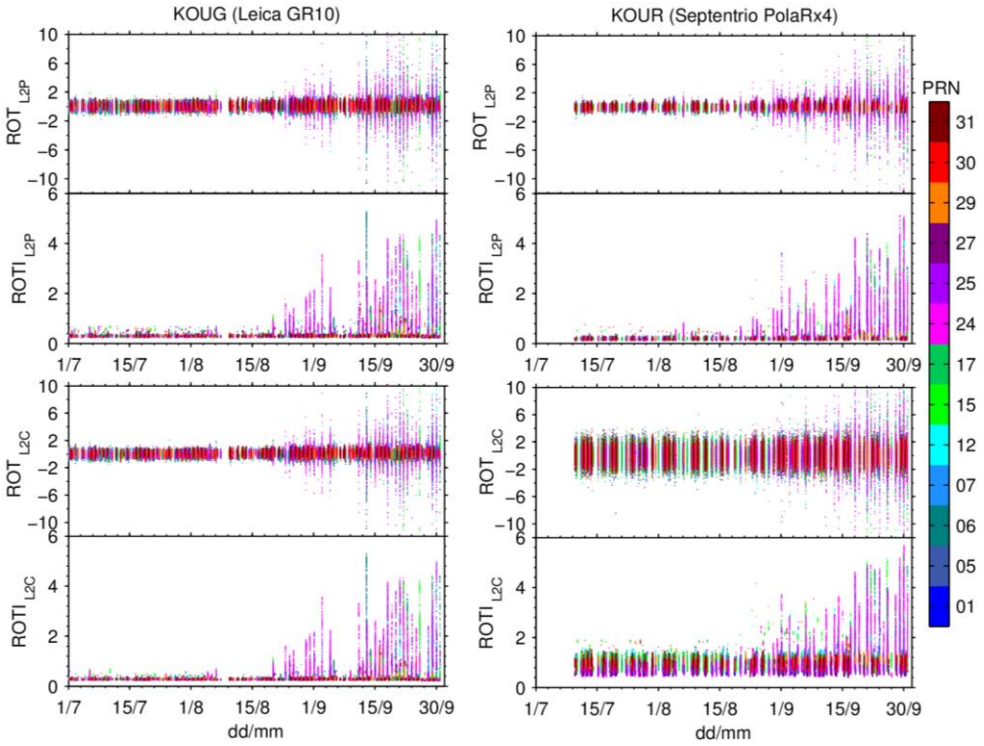

Fig. 7 ROT and ROTI time series derived from GPS data of modernized satellites collected by two adjacently installed GNSS receivers at KOUG station (left column) and KOUR station (right column) in the period of July 1 to September 30, 2014. The unit of ROT and ROTI is TECu/min. The receiver types of KOUG and KOUR stations are Leica GR10 and Septentrio PolaRx4, respectively.

For the ROT_{L2C} and $ROTI_{L2C}$, the KOUR station however shows a much larger magnitude than the KOUG station, as shown in Figure 7. The ROT_{L2C} and $ROTI_{L2C}$ at the KOUR station generally vary in the ranges of -4 to 4 TECu/min and -0.5 to 1.6 TECu/min, respectively. In comparison, the ROT_{L2C} and $ROTI_{L2C}$ at the KOUG station are in the ranges of -1.2 to 1.2 TECu/min and 0.2 to 0.4 TECu/min, respectively. The KOUR station is equipped with a Septentrio PolaRx4 receiver, which is from the same GNSS receiver family as the Septentrio PolaRxS Pro receiver installed at the HKHT station in Hong Kong. This explains why the KOUR station has a result very similar to that of HKHT station. Instead, KOUG is equipped with a Leica GR10 receiver. This implies that receiver type is a possible factor that affects the values of ROT_{L2C} and $ROTI_{L2C}$. Table 1 indicates that the Leica GR10 receiver at the KOUG station and the Septentrio PolaRx4 receiver at the KOUR station deliver two different types of L2C signals. The Leica GR10 receiver outputs L2C (M) and the Septentrio PolaRx4 receiver outputs L2C (L) signal. Thus it is speculated that the different types of L2C measurements result in the differences in the ROT_{L2C} and $ROTI_{L2C}$ values of the two stations. To verify this, we continue to

analyze the ROT_{L2C} and $ROTI_{L2C}$ values obtained from another two collocated MGEX stations SIN0 and SIN1. The result from these two stations, presented in the later section, will show that the differences of ROT_{L2C} and $ROTI_{L2C}$ values may be related to the GNSS receiver type, i.e., receiver configurations, but not the type of L2C measurements.

The ($ROTI_{L2C}$-$ROTI_{L2P}$) values for the KOUG and KOUR stations over the study period are summarized in the form of histogram and displayed in Figure 8 and Figure 9, respectively. It can be clearly seen from Figure 8 that for the KOUG station the ($ROTI_{L2C}$-$ROTI_{L2P}$) of each modernized satellite has an approximately Gaussian distribution within the range of -0.1~0.1 TECu/min, with a mean value in the range of -0.022 to -0.009 TECu/min.

Unlike the KOUG station, the KOUR station shows a significant overestimation of $ROTI_{L2C}$ as depicted in Figure 9. The distribution of ($ROTI_{L2C}$-$ROTI_{L2P}$) is severely shifted to the right side. The ($ROTI_{L2C}$-$ROTI_{L2P}$) varies in the range of 0~2 TECu/min, with a mean in the range of 0.47~0.88 TECu/min for all the satellites. As noted from Figure 4 and Figure 9, the distribution pattern for the KOUR station is also very similar to that for the HKHT station. Both the KOUR and HKHT stations have the Septentrio receivers installed, suggesting a consistent overestimation of ROT_{L2C} by the same type of receiver.

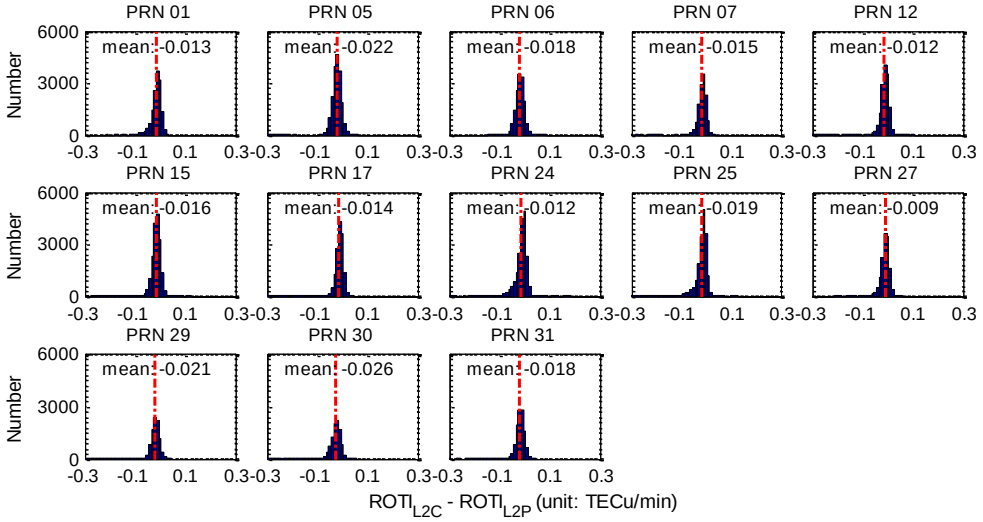

Fig. 8 Histogram of ($ROTI_{L2C}$-$ROTI_{L2P}$) of each modernized GPS satellite observed by the Leica GR10 GNSS receiver at the KOUG station in the period of July 1 to September 30, 2014.

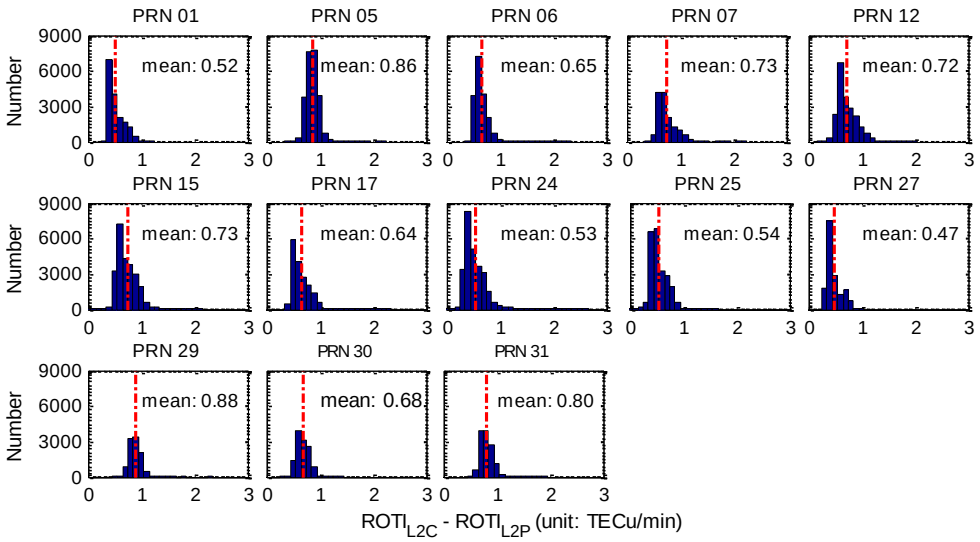

Fig. 9 Histogram of ($ROTI_{L2C}$-$ROTI_{L2P}$) of each modernized GPS satellite observed by the Septentrio PolaRx4 GNSS receiver at the KOUR station in the period of July 1 to September 30, 2014.

In order to have a further understanding of the L2C signal properties, the ROT_{L2C} and $ROTI_{L2C}$ values at two more MGEX stations, which are equipped with different types of receiver but output the same type of L2C (M+L) measurements, are studied. The two MGEX stations, SIN0 and SIN1, are equipped with a Javad TRE-G3TH DELTA and a Trimble NetR9 receiver, respectively. Both Javad and Trimble receivers output the same type of L2C (M+L) measurements. The ROT and ROTI results are illustrated in Figure 10. Compared with those observed at the HKHT, KOUG and KOUR stations shown in Figure 3 and Figure 7, large ROT and ROTI values are more frequently seen at the SIN0 and SIN1 stations, especially in September 2014. This can be attributed to their locations that are very close to the equator as shown in Figure 1 and Table 1. Though the two receivers are connected to a common antenna, they however have different ROT and ROTI. At the SIN0 station, the ROT_{L2P} and $ROTI_{L2P}$ are generally in the range of -2~2 TECu/min and 0.4 to 1.6 TECu/min, respectively; the ROT_{L2C} and $ROTI_{L2C}$ values are in the ranges -1.2~1.2 TECu/min and 0.4~1.2 TECu/min, respectively. At the SIN1 station, however, the two types of ROT are at the same level of -2~2 TECu/min. Similarly the $ROTI_{L2C}$ and $ROTI_{L2P}$ at the SIN1 station are very similar, at the level of 0.4~0.5 TECu/min. As shown in Table 1, the SIN0 and SIN1 stations output the same type of L2C (M+L) measurements from two different types of receivers (Javad and Trimble). However, their ROT_{L2C} and $ROTI_{L2C}$ are significantly different, as shown in Figure 10. This clearly suggests that the differences in the ROT_{L2C}, observed at the SIN0 and SIN1 stations, are related to the GNSS receiver configurations. So are the $ROTI_{L2C}$ differences.

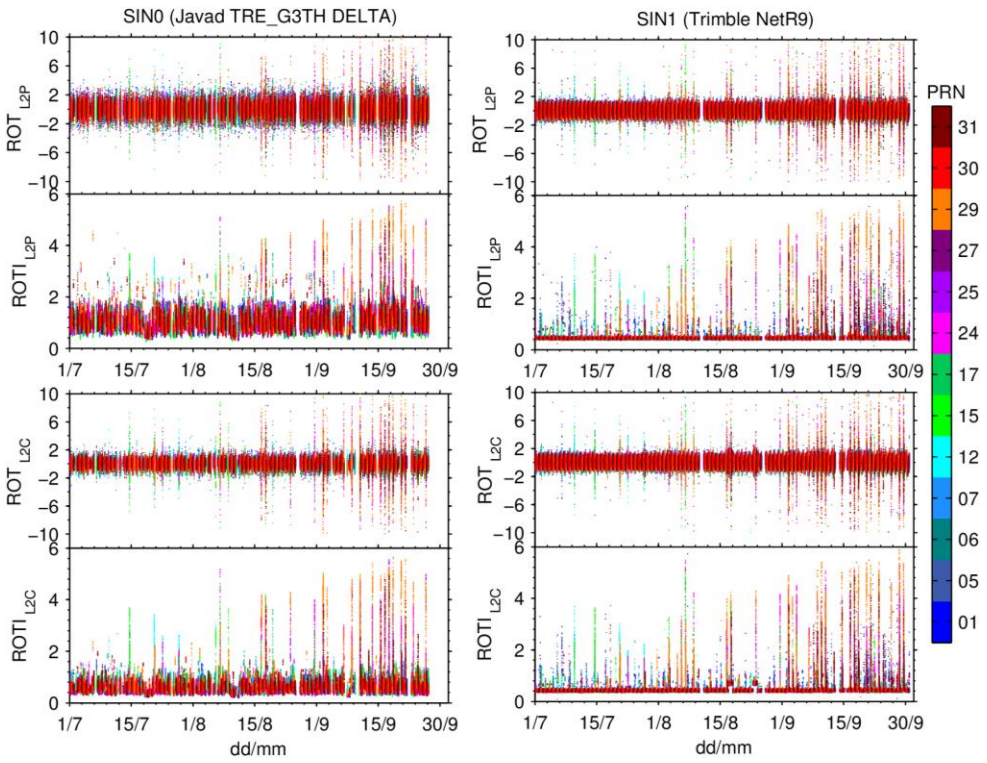

Fig. 10 ROT and ROTI time series derived from GPS data of the modernized satellites collected by two collocated GNSS receivers at SIN0 station (left column) and SIN1 station (right column) in the period of July 1 to September 30, 2014. The unit of ROT and ROTI is TECu/min. The receiver types of SIN0 and SIN1 are Javad TRE-G3TH DELTA and Trimble NetR9, respectively.

A quantitative analysis is also conducted to show the ($ROTI_{L2C}$-$ROTI_{L2P}$) for the SIN0 and SIN1 stations, which are displayed in Figure 11 and Figure 12, respectively. The SIN0 station with the receiver type of Javad TRE-G3TH DELTA shows an underestimation of $ROTI_{L2C}$ with respect to the $ROTI_{L2P}$. The mean ($ROTI_{L2C}$-$ROTI_{L2P}$) of each modernized GPS satellite is generally in the range of -0.495 to -0.338 TECu/min. The SIN1 station with the receiver type of Trimble NetR9 shows an approximately Gaussian distribution of ($ROTI_{L2C}$-$ROTI_{L2P}$) within the range of -0.1 to 0.1 TECu/min, a mean value about 0 TECu/min for each modernized GPS satellite. The Trimble receiver's ($ROTI_{L2C}$-$ROTI_{L2P}$) result is very similar to that at the KOUR station equipped with a Leica GR10 receiver as shown in Figure 8.

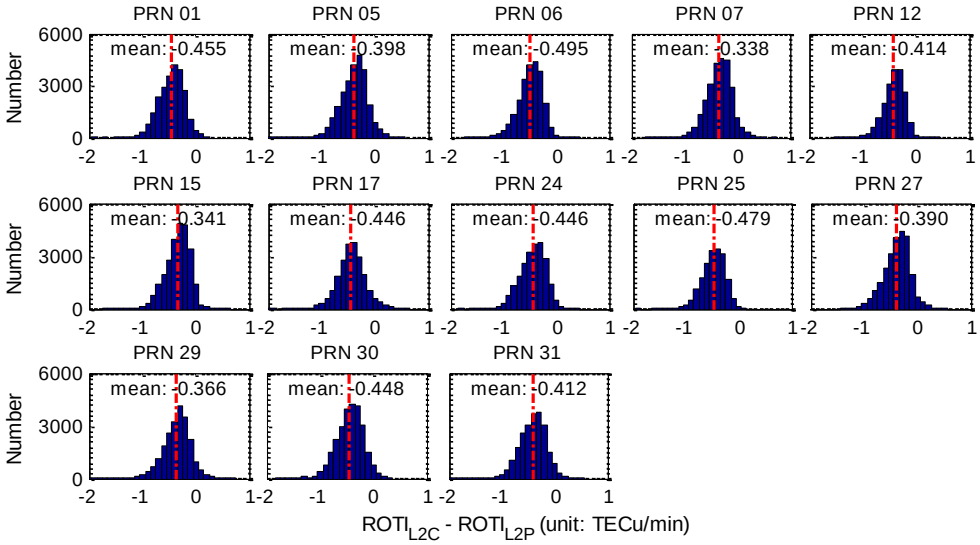

Fig. 11 Histogram of (ROTI$_{L2C}$-ROTI$_{L2P}$) of each modernized satellite observed by the Javad TRE-G3TH DELTA GNSS receiver at the SIN0 station in the period of July 1 to September 30, 2014.

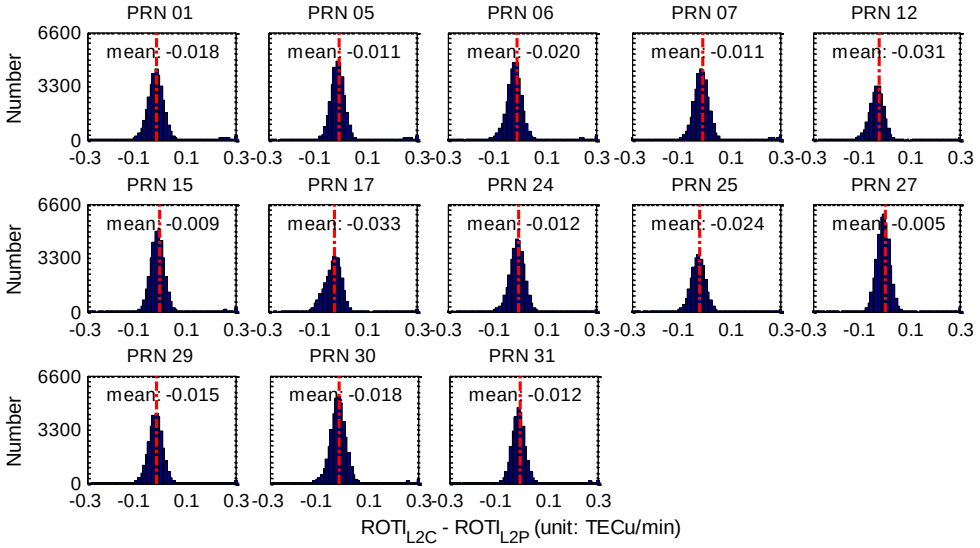

Fig. 12 Histogram of (ROTI$_{L2C}$-ROTI$_{L2P}$) of each modernized satellite observed by the Trimble NetR9 GNSS receiver at the SIN1 station in the period of July 1 to September 30, 2014.

Discussion

The above analysis presents the performance of L2C measurements in deriving ROT and ROTI parameters using GPS data from four types of GNSS receivers, i.e., Javad, Leica, Septentrio and Trimble, deployed at low-latitude regions. Two types of ROTI indices, ROTI$_{L2P}$ and ROTI$_{L2C}$, are

calculated using the L1 C/A and L2 P(Y) measurements and the L1 C/A and L2C measurements, respectively. The magnitude of $ROTI_{L2C}$ of each type of GNSS receiver is quite different from the $ROTI_{L2P}$, as shown in Figures 3, 7 and 10. For a better comparison, the mean values of ($ROTI_{L2C}$-$ROTI_{L2P}$) corresponding to each modernized GPS satellite observed at each station, which have been shown in Figures 4, 8, 9, 11 and 12, are summarized in Figure 13. For the Septentrio receivers installed at the HKHT and KOUR stations, the $ROTI_{L2C}$ is significantly larger than the $ROTI_{L2P}$ by 0.5 to 1.1 TECu/min on average, depending on individual GPS satellite. However, for the Javad receiver at the SIN0 station, the $ROTI_{L2C}$ is significantly smaller than the $ROTI_{L2P}$ by 0.3~0.5 TECu/min on average, also depending on individual GPS satellite. For the Leica and Trimble receivers at KOUG and SIN1 stations, the differences between $ROTI_{L2C}$ and $ROTI_{L2P}$ are negligible. From Figure 13, it can be found that with the same type of L2C(L) measurements, a common feature of overestimation of $ROTI_{L2C}$ is observed by the Septentrio receivers at HKHT and KOUR stations (also refer to Figures 3 and 7). But it is also observed that even with the same type of L2C(M+L) measurements, there are distinctively different feature of ($ROTI_{L2C}$-$ROTI_{L2P}$) for the Javad and Trimble receivers collocated at SIN0 and SIN1 stations (also refer to Figure 10). These results suggest the relationship between $ROTI_{L2C}$ and $ROTI_{L2P}$ depends on the receiver configurations, instead of the type of L2C measurements.

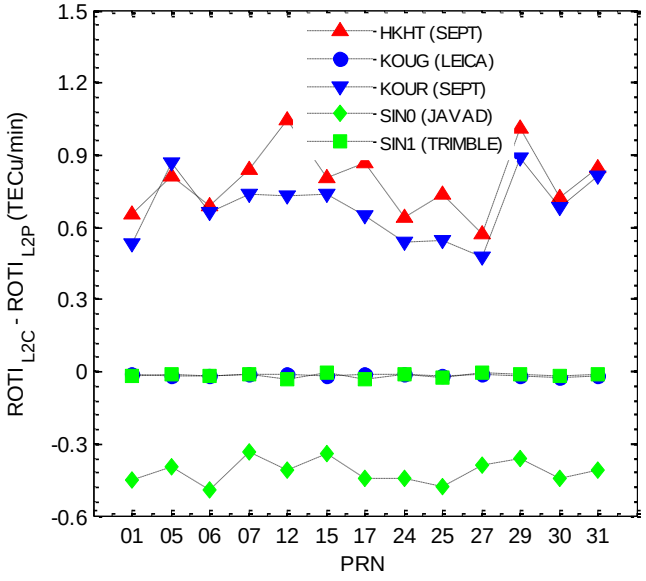

Fig. 13 Average differences between $ROTI_{L2C}$ and $ROTI_{L2P}$ observed by each modernized GPS satellite by five different types of GNSS receivers over the study period July 1 to September 30, 2014

As a further illustration, a cross-comparison of the $ROTI_{L2C}$ as well as $ROTI_{L2P}$ between the two receivers at zero/short baselines over the study period is made based on the datasets shown in Figures 7 and 10. The average differences of ROTI are summarized in Figure 14. It can be seen that the $ROTI_{L2P}$ between two receivers at zero/short baselines have non-negligible differences, so does $ROTI_{L2C}$. For the Leica and Septentrio receivers with a short baseline at KOUG and KOUR stations, the difference of legacy $ROTI_{L2P}$ is in the range of -0.19 to -0.11 TECu/min while the $ROTI_{L2C}$ discrepancy is much larger, varying between 0.3 and 0.8 TECu/min. Noticeably, at the collocated SIN0 and SIN1 stations the Javad and Trimble receivers have $ROTI_{L2P}$ differences in the range of 0.4~0.8 TECu/min, but $ROTI_{L2C}$ differences less than 0.4 TECu/min. The results summarized in Figures 13 and 14 indicate that two receivers of different types at a short baseline or even two collocated stations estimate ROTI (both $ROTI_{L2C}$ and $ROTI_{L2P}$) quite differently. In Figure 13 and Figure 14, it is also noted that the discrepancy of ROTI varies differently among modernized GPS satellites. As seen from Figure 15, which shows the maximum elevation of each modernized satellite tracked by each station, large discrepancy is observed for satellites with low elevation angles, indicating that the ROTI have poor consistencies at low satellite elevation angles, especially for the Javad and Septentrio receivers.

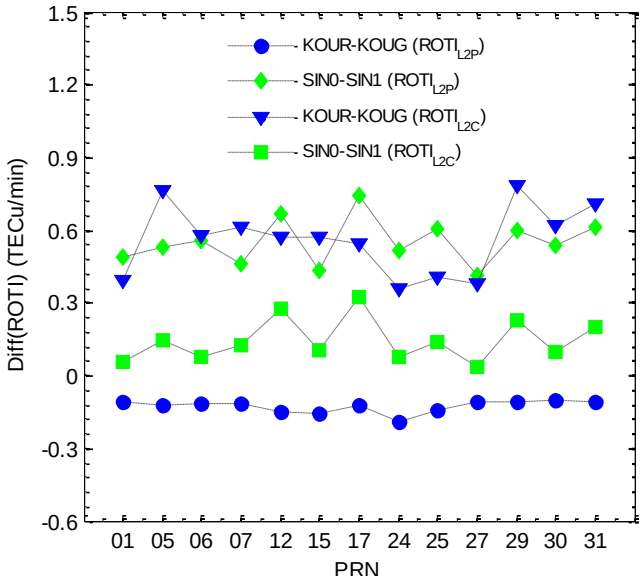

Fig. 14 Average differences between the ROTIs derived from the pair of KOUG and KOUR stations, as well as the pair of SIN0 and SIN1 stations over the studied period July 1 to September 30, 2014

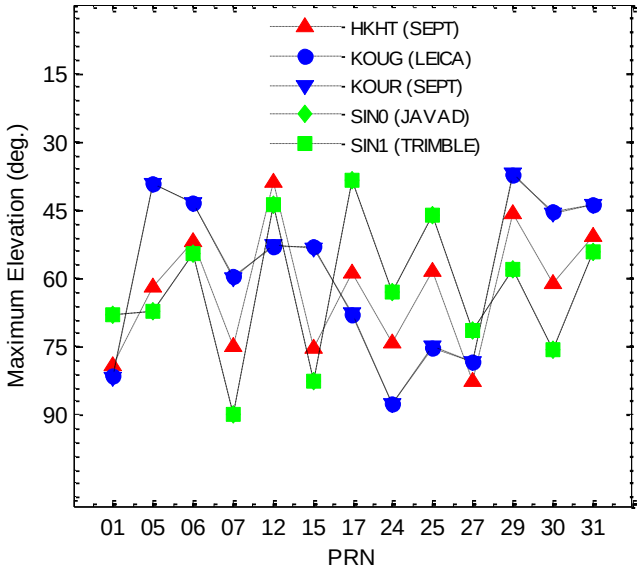

Fig. 15 The maximum elevation of each modernized GPS satellite tracked by each station during the study period July 1 to September 30, 2014

Three types of L2C measurements, i.e., L2C(M), L2C(L) and L2C(M+L) from different types of receivers are used in this study. The result of this study indicates that these three kinds of L2C tracking modes have inconsistent performance when used to estimate ROTI and this inconsistency depends on the receiver types. Different types of GNSS receivers differ from each other in their configurations, such as tracking techniques (Humphreys et al. 2008). Different manufacturers are likely to have different front-end and standard correlator implementations (Hauschild and Montenbruck 2014). The diversified tracking techniques employed by various receivers may contribute to the inconsistent performance of L2C measurements when they are used to calculate ROTI.

ROTI is a good parameter to indicate the occurrence of ionospheric irregularities or scintillation activity (Pi et al. 1997). Taking advantage of the ground-based GNSS receiver network, the ROTI has been used to investigate the generation, evolution and decay phases of ionospheric irregularities and associated scintillation (Krankowski et al. 2006; Pi et al. 2013; Cherniak et al. 2014). Thus, the numerical value of ROTI is of importance since it can be used to signify the occurrence characteristics of ionospheric irregularities. $ROTI_{L2P}$ >0.5 TECu/min, when derived from the GPS legacy signals, can represent ionospheric irregularities at scale length of a few kilometers (Ma and Maruyama 2006). The difference between daytime $ROTI_{L2P}$ and nighttime $ROTI_{L2P}$ with a threshold of 0.075 TECu/min can detect the occurrence of ionospheric irregularities (Nishioka et al. 2008). In this study, it shows that the ROTI derived from L2C measurements, i.e. $ROTI_{L2C}$, may dramatically differ from the legacy $ROTI_{L2P}$,

even using data from the same single GNSS receiver. The ($ROTI_{L2C}$-$ROTI_{L2P}$) can be as large as 0.6 to 0.9 TECU/min, as shown by the two Septentrio receivers in Figure 13, which is significantly higher than the previously used thresholds. Among different types of receivers, the $ROTI_{L2C}$ is different even if the receivers are placed close enough or even connected with the same GNSS antenna, so does the $ROTI_{L2P}$. So cares must be taken if (1) the new civilian L2C measurements are used to calculate the $ROTI_{L2C}$ index to avoid mixing with the $ROTI_{L2P}$; (2) different types of GNSS receivers are simultaneously used to calculate $ROTI_{L2P}$ (or $ROTI_{L2C}$) to study ionospheric irregularities. The inconsistency between $ROTI_{L2P}$ and $ROTI_{L2C}$ of the same receiver, or the inconsistency between two $ROTI_{L2P}$ (or $ROTI_{L2C}$) values of two different types of receivers, even when closely placed or collocated, requires us to be very cautious when ROTI index is derived to characterize ionospheric irregularities and scintillations.

It should be mentioned that in the above data analysis, the results are derived from data recorded in 2014. In order to verify whether the characteristics of L2C measurements recorded by different receivers vary with time or with the latest update of GNSS receiver firmware, the latest data recorded in 2016 by the same GNSS stations are analyzed. Consistent results have been obtained but not shown here due to length limitation. This implies that the characteristics of L2C measurements do not change with time or with the update of receiver firmware.

Conclusions

In this study, the performance of L2C measurements in characterizing ionospheric irregularities and associated scintillations at low-latitude regions is investigated, by studying the $ROTI_{L2P}$ and $ROTI_{L2C}$ indices. Dual-frequency GPS data collected from a GNSS-based Septentrio PolaRxS Pro ionospheric scintillation monitoring receiver in Hong Kong and four different types of GNSS receivers in the MGEX network in the period of July 1 to September 30, 2014 are used in the analysis.

For each type of GNSS receiver, the derived $ROTI_{L2P}$ and $ROTI_{L2C}$ indices have different magnitudes. The Javad TRE-G3TH DELTA receiver tends to underestimate the $ROTI_{L2C}$ with respect to $ROTI_{L2P}$. Instead, the Septentrio type receivers (both Septentrio PolaRxS Pro and Septentrio PolaRx4) overestimate the $ROTI_{L2C}$ with respect to $ROTI_{L2P}$. Nevertheless, the $ROTI_{L2C}$ data from both Leica GR10 and Trimble NetR9 receivers agree with their $ROTI_{L2P}$ very well. In the cross-comparison of ROTI between two receivers at zero/short baselines, the inconsistency of two sets of $ROTI_{L2C}$

between two closely spaced receivers or two collocated receivers is significant, so does $ROTI_{L2P}$. Large inconsistency is found to be related with modernized GPS satellites with the low maximum elevation angle. The correlation analysis suggests the correlation coefficient for $ROTI_{L2C}$ and S_4 is comparable to that for $ROTI_{L2P}$ and S_4, but the ratio of $ROTI_{L2C}/S_4$ is larger than that of $ROTI_{L2C}/S_4$. It is speculated various tracking techniques adopted by different receivers contribute to the inconsistent results between $ROTI_{L2C}$ and $ROTI_{L2P}$. This study can contribute to the community, particularly the ionosphere and space weather community, by reminding researchers of carefully using $ROTI_{L2C}$ and $ROTI_{L2P}$ when the ROTI are from multiple types or even a single type of GNSS receiver are adopted to study ionospheric irregularities and scintillations.

Acknowledgments

The supports from the National Natural Science Foundation of China (Grant No. 41274039) are gratefully acknowledged. This work is supported by the Hong Kong Research Grants Council (RGC) projects (PolyU 5325/12E, F-PP0F and PolyU 5203/13E, B-Q37X) and PolyU project 4-BCBT and G-YBDA. We thank the International GNSS Service's Crustal Dynamics Data Information System (CDDIS) for providing the MGEX data. The anonymous reviewers are thanked for providing constructive comments, which help improve the quality of this paper.

References

Al-Fanek O, Skone S, Lachapelle G, Fenton P (2007) Evaluation of L2C Observations and Limitations. In: Proceedings of the ION GNSS, Fort Worth, Texas, 25-28 September 2007. pp 2510-2518

Basu S, Groves K, Quinn J, Doherty P (1999) A comparison of TEC fluctuations and scintillations at Ascension Island. Journal of Atmospheric and Solar-Terrestrial Physics 61 (16):1219-1226

Beach TL, Kintner PM (1999) Simultaneous Global Positioning System observations of equatorial scintillations and total electron content fluctuations. Journal of Geophysical Research: Space Physics (1978–2012) 104 (A10):22553-22565

Cherniak I, Zakharenkova I, Krankowski A (2014) Approaches for modeling ionosphere irregularities based on the TEC rate index. Earth, Planets and Space 66 (1):1-5. doi:10.1186/s40623-014-0165-z

Engel U (2008) A theoretical performance analysis of the modernized GPS signals. In: Position, Location and Navigation Symposium, 2008 IEEE/ION, Monterey, CA, 5-8 May 2008. pp 1067-1078

512 Fontana RD, Cheung W, Stansell T (2001) The modernized L2 civil signal. GPS world 12 (9):28-35
513 Hauschild A, Montenbruck O (2014) A study on the dependency of GNSS pseudorange biases on correlator
514 spacing. GPS Solutions 20 (2):159-171. doi:10.1007/s10291-014-0426-0
515 Humphreys T, Young L, Pany T (2008) Considerations for Future IGS Receivers. In: IGS Analysis Center
516 Workshop, Miami Beach, FL, 2-6 June 2008. pp 1-19
517 Krankowski A, Shagimuratov I, Baran L, Ephishov I, Tepenitzyna N (2006) The occurrence of polar cap patches
518 in TEC fluctuations detected using GPS measurements in southern hemisphere. Advances in Space
519 Research 38 (11):2601-2609
520 Leandro RF, Thirumurthi T, Sukeova L, Langley RB, Santos MC (2008) Analysis of GPS L2C signal quality
521 and its impact on PPP performance. In: Proceedings of the 2008 National Technical Meeting of The
522 Institute of Navigation, San Diego, California, 28–30 January 2008. pp 1020-1031
523 Leick A, Rapoport L, Tatarnikov D (2015) GPS satellite surveying. John Wiley & Sons. doi:DOI:
524 10.1002/9781119018612
525 Leveson I (2006) Benefits of the New GPS Civil Signal. Inside GNSS 1 (5):42-47
526 Li H, Lu M (2015) Double-chipwise correlation technique for efficient L2C signal acquisition. Aerospace and
527 Electronic Systems, IEEE Transactions on 51 (2):1575-1582
528 Liu Z (2011) A new automated cycle slip detection and repair method for a single dual-frequency GPS receiver.
529 Journal of Geodesy 85 (3):171-183
530 Ma G, Maruyama T (2006) A super bubble detected by dense GPS network at east Asian longitudes.
531 Geophysical research letters 33 (21). doi:10.1029/2006GL027512
532 Marques H, Monico J, Marques H (2015) Performance of the L2C civil GPS signal under various ionospheric
533 scintillation effects. GPS Solutions 20 (2):139-149. doi:10.1007/s10291-015-0472-2
534 McDonald KD (2002) The modernization of GPS: plans, new capabilities and the future relationship to Galileo.
535 Journal of Global Positioning Systems 1 (3):1-17
536 Montenbruck O, Hauschild A, Steigenberger P (2014a) Differential Code Bias Estimation using Multi-GNSS
537 Observations and Global Ionosphere Maps. Navigation 61 (3):191-201
538 Montenbruck O, Steigenberger P, Khachikyan R, Weber G, Langley R, Mervart L, Hugentobler U (2014b) IGS-
539 MGEX: preparing the ground for multi-constellation GNSS science. Inside GNSS 9 (1):42-49
540 Nishioka M, Saito A, Tsugawa T (2008) Occurrence characteristics of plasma bubble derived from global
541 ground-based GPS receiver networks. Journal of Geophysical Research 113 (A05301).
542 doi:10.1029/2007JA012605
543 O'Keefe K, Wang D, Petovello MG, Gernot C (2009) Benefit of Partial L2C Availability for Correcting
544 Ionospheric Error for Standalone GPS. In: The 22nd International Meeting of the Satellite Division of
545 the Institute of Navigation, Savannah, GA, 22-25 September 2009. pp 2530 - 2550

546 Oladipo O, Schüler T (2013) Equatorial ionospheric irregularities using GPS TEC derived index. Journal of
547 Atmospheric and Solar-Terrestrial Physics 92:78-82
548 Pi X, Mannucci A, Lindqwister U, Ho C (1997) Monitoring of global ionospheric irregularities using the
549 worldwide GPS network. Geophysical Research Letters 24 (18):2283-2286
550 Pi X, Mannucci AJ, Valant-Spaight B, Bar-Sever Y, Romans LJ, Skone S, Sparks L, Hall GM (2013)
551 Observations of global and regional ionospheric irregularities and scintillation using GNSS tracking
552 networks. In: Proceedings of the ION 2013 Pacific PNT Meeting, Honolulu, Hawaii, April 23-25 2013.
553 pp 752-761
554 Rizos C, Montenbruck O, Weber R, Weber G (2013) The IGS MGEX experiment as a milestone for a
555 comprehensive multi-GNSS service. In: Proceedings of the ION 2013 Pacific PNT Meeting, Honolulu,
556 Hawaii, 23-25 April 2013. pp 289 - 295
557 Shanmugam S, Jones J, MacAulay A, Van Dierendonck A (2012) Evolution to modernized GNSS ionoshperic
558 scintillation and TEC monitoring. In: Position Location and Navigation Symposium, 2012 IEEE/ION,
559 23-26 April 2012. pp 265-273
560 Sokolovskiy S, Schreiner W, Zeng Z, Hunt D, Kuo Y-H, Meehan T, Stecheson T, Mannucci A, Ao C (2014)
561 Use of the L2C signal for inversions of GPS radio occultation data in the neutral atmosphere. GPS
562 Solutions 18 (3):405-416
563 Sükeová L, Santos MC, Langley RB, Leandro RF, Nnani O, Nievinski F (2007) GPS L2C signal quality analysis.
564 In: Proceedings of the ION 63rd Annual Meeting, Cambridge, MA, 23 - 25 April 2007. pp 23-25
565 Tiwari R, Strangeways H, Tiwari S, Ahmed A (2013) Investigation of ionospheric irregularities and scintillation
566 using TEC at high latitude. Advances in Space Research 52 (6):1111-1124
567 Tran M (2004) Performance evaluations of the new GPS L5 and L2 Civil (L2C) signals. Navigation 51 (3):199-
568 212
569 Wang D, O'Keefe K (2010) Benefit of partial L2C availability to estimate ionospheric delay for dual-frequency
570 GPS ambiguity resolution. In: Position Location and Navigation Symposium, 2010 IEEE/ION, 2010. pp
571 44-52
572 Wang N, Yuan Y, Li Z, Montenbruck O, Tan B (2016) Determination of differential code biases with multi-
573 GNSS observations. Journal of Geodesy 90 (3):209-228. doi:10.1007/s00190-015-0867-4
574 Yang Z, Liu Z (2015) Correlation between ROTI and Ionospheric Scintillation Indices using Hong Kong low-
575 latitude GPS data. GPS Solutions:1-10. doi:10.1007/s10291-015-0492-y
576
577
578

Author biographies

Zhe Yang currently is a Ph.D. student at the Department of Land Surveying and Geo-Informatics (LSGI), the Hong Kong Polytechnic University, Hong Kong, P. R. China. She received the B.S. degree in surveying engineering from the Central South University, Hunan, China, in 2010 and the Master degree in Astrometry and Celestial Mechanics from Shanghai Astronomical Observatory (SHAO), Chinese Academy of Sciences (CAS) in 2013. Her research interests include GNSS ionospheric scintillation, ionospheric models and GNSS ionospheric tomography.

Zhizhao Liu currently is an Associate Professor at the Department of Land Surveying and Geo-Informatics (LSGI), the Hong Kong Polytechnic University, Hong Kong, P. R. China. He is the founder of the Micro-Laboratory of Atmospheric Research and Geomatics Engineering (Micro-LARGE) at the LSGI, which aims to develop innovative methods and algorithms for GNSS Precise Point Positioning, GNSS positioning and navigation under challenging conditions, ionosphere modeling and scintillation monitoring, and tropospheric modeling & GNSS meteorology. He received his B.Sc. degree in Surveying Engineering from the Jiangxi University of Science and Technology, China, in 1994 and M.Sc. degree in Geodesy from the Wuhan University, China, in 1997. He received Ph.D. degree in Geomatics Engineering from the University of Calgary, Canada, in 2004.

602